A modification to dense sand dynamic simulation capability of Pastor–Zienkiewicz–Chan model

Amin Iraji, Orang Farzaneh & Ehsan Seyedi Hosseininia

Acta Geotechnica

ISSN 1861-1125
Volume 9
Number 2

Acta Geotech. (2014) 9:343-353
DOI 10.1007/s11440-013-0291-y

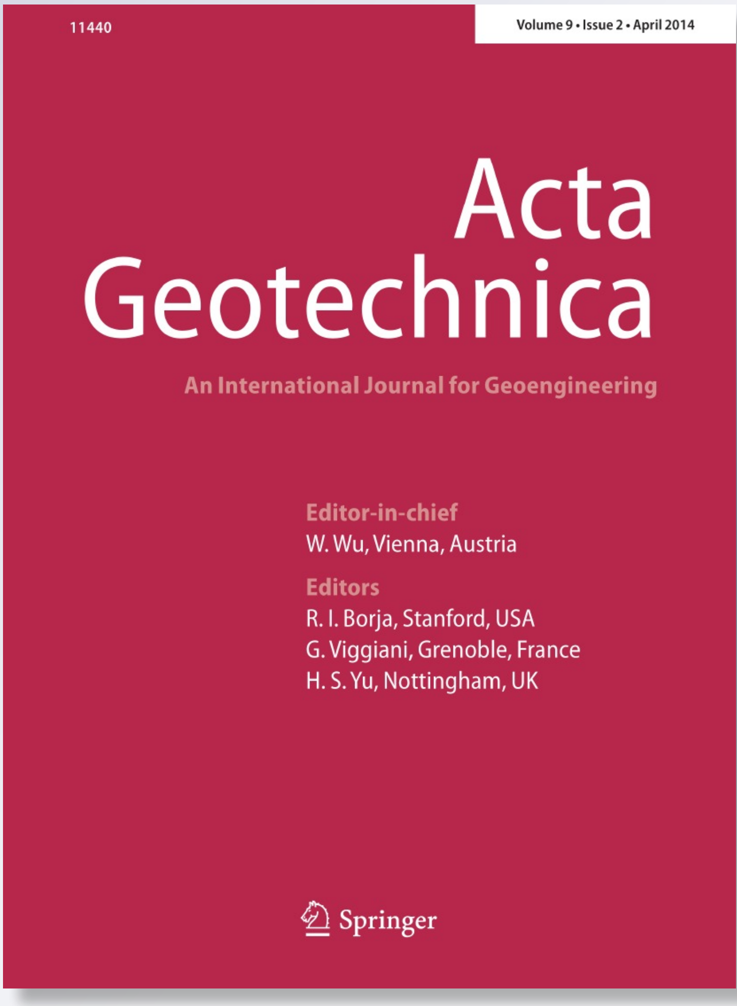

Springer

Acta Geotechnica (2014) 9:343–353
DOI 10.1007/s11440-013-0291-y

SHORT COMMUNICATION

A modification to dense sand dynamic simulation capability of Pastor–Zienkiewicz–Chan model

Amin Iraji · Orang Farzaneh · Ehsan Seyedi Hosseininia

Received: 25 January 2013 / Accepted: 28 October 2013 / Published online: 14 December 2013

Abstract A modification to the nonlinear Pastor–Zienkiewicz–Chan (PZC) constitutive model without any change in the number of model parameters is introduced in order to simulate stiffness degradation of dense sands at dynamic loading. The PZC model is based on generalized plasticity and was verified by good prediction of liquefaction and undrained behavior of saturated sand. The PZC is a robust model that can predict drained dynamic behavior of sands, especially stiffness increase in loose sand at reloading of dynamic loading. Yet, this model does not show stiffness degradation of dense sand at reloading. The modification is made through modifying the stress memory factor, H_{DM}, which is multiplied by the plastic modulus, H_L. This modification does not influence reloading behavior of loose sand. The modified PZC model is verified via results of drained cyclic tests. Two cyclic triaxial tests on loose and dense specimens, along with two cyclic plane strain tests on dense sand are utilized for validation. The model simulation shows that the modified PZC model is able to predict the stiffness degradation of dense sand at reloading well.

Keywords Constitutive model · Dense sand · Dynamic simulation · Reloading · Stress memory factor

A. Iraji (✉) · O. Farzaneh
School of Civil Engineering, University of Tehran, Tehran, Iran
e-mail: a.iraji@ut.ac.ir

O. Farzaneh
e-mail: Ofarzane@ut.ac.ir

E. S. Hosseininia
School of Civil Engineering, Ferdowsi University of Mashhad, Mashhad, Iran
e-mail: eseyedi@um.ac.ir

1 Introduction

The generalized plasticity is a well-established nonlinear framework of plasticity that has been formulated without thermodynamic considerations and recourse to yield or potential surfaces. These features bear some resemblance to hypoplasticity, which is based on nonlinear tensorial functions. Hypoplasticity provides an interesting alternative approach to capture the complex behavior during cyclic loadings [27]. The hypoplasticity theory was first introduced by Kolymbas [15]. The general formulation of hypoplasticity as nonlinear tensor functions was proposed by Wu and Kolymbas [45]. An exhaustive review on hypoplasticity was given by Wu and Kolymbas [46]. This theory was originally developed to predict the behavior of granular materials such as sand or gravel. A major contribution was made by Wu et al. [47] to introduce critical state into hypoplastic model by including void ratio as an additional state variable. Gudehus [12] presented a comprehensive hypoplastic model and subsequently improved it using viscous effects [13]. The hypoplastic constitutive laws were widely used at Karlsruhe University [14, 16, 29, 42, 43, 44] and at Grenoble University [3, 4, 7–9, 17]. Recently, the hypoplastic models have been extended to cohesive soils. Niemunis [28] introduced a rate-dependent visco-hypoplastic model for clays. Herle and Kolymbas [14] modified the model by predicting the rate-independent behavior of soils with low friction angles. Mašín [22] developed the latter model through reducing the number of parameters while improving fine-grained soil behavior. Other more recent developments have also been made for hypoplastic models. Osinov [30] used an extended hypoplastic model for the cyclic deformation of granular soils with the purpose of analyzing soil liquefaction around a vibrating pile toe. Mašín [23] developed a hypoplasticity model for clay with explicitly defined asymptotic states. Fuentes et al. [11] introduced a hypoplastic model for cyclic behavior of sand with the incorporation of a loading surface. Zhang and Wang [48] employed a bounding surface hypoplasticity model for predicting post-liquefaction deformation of saturated sand under undrained cyclic loading.

On the other hand, generalized plasticity theory was introduced by Mroz and Zienkiewicz [26] and Zienkiewicz and Mroz [51] and was extended by Zienkiewicz et al. [52] and Pastor et al. [31–33]. This model is able to reproduce the behavior of dense and loose sands under quasi-static and dynamic loading. In the generalized plasticity theory, the yield surface and plastic potential are not explicitly defined. Instead, direction vectors are used. By applying true laws to the direction of plastic flow, loading–unloading directions and plastic moduli, reasonable behavior of soil can be predicted. Thus, generalized plasticity provides a relatively simple framework for the prediction of geomaterials behavior under different loading conditions [18]. Pastor, Zienkiewicz and Chan [33] developed this model to a perfect level in *p*-*q* triaxial space. This model was utilized for liquefaction and undrained simulation of saturated sand successively.

Several modifications to the generalized plasticity model have been proposed. Pastor et al. [34] implemented anisotropy effect to the model. Sassa and Sekiguchi [37] considered the effects of principle stress rotation, and Bahda et al. [1] introduced a slightly different version of the generalized plasticity model by employing a new state parameter and double hardening rules. Zhang et al. [49] developed generalized plasticity for use in partially saturated soils by means of implicit integration method. In other studies, shear-band-dominated process was simulated in fully saturated and partially saturated sand by means of dynamic strain localization and multiphase material model with adaptation of the generalized plasticity in computational process [38, 50]. On the issue of the generalized plasticity for unsaturated soils, Bolzon et al. [2] proposed a model on the basis of the definition of the effective stress tensor. This model was subsequently extended by Tamagnini and Pastor [39] using the same approach that was introduced by Bolzon et al. [2]. Later, modification was done by Santagiuliana and Schrefler [36]. Ling and Liu [18] extended the generalized plasticity to include pressure dependency as well as densification behavior of sand under monotonic and cyclic loading. Merodo et al. [10] presented an enhanced generalized plasticity that is able to reproduce damage phenomena in geomaterials. Ling and Yang [19] also extended this model using a nonlinear critical state line. They modified the plastic modulus, loading vectors and plastic flow direction vectors, which are dependent on the state parameter. This model includes 12 and 17 constants for simulation of monotonic and dynamic loading, respectively. Tonni et al. [41] developed the basic generalized plasticity by introducing a state-dependent dilatancy and adjusting plastic modulus via developments on isotropic compression and modeling softening of dense sands. The latter work was done with the aim of improving the prediction of silty soil behavior. Other developments on this issue were employed by Cola and Tonni [5] and Cola et al. [6]. Liu and Ling [20] used the modified generalized plasticity for soil-structure interface subjected to dynamic loading. The critical state soil mechanics was modified to describe soil-particle breakage and also degradation during cyclic shearing. Mira et al. [25] introduced contribution of hyperelastic formulation to explain reversible component of the soil response instead of hypoelastic formulation that was introduced in the original model. Manzanal et al. [21] modified the generalized plasticity by reformulation of flow rule, loading–unloading discriminating direction and plastic modulus, which are dependent on state parameter.

Loose sand and dense sand show different behaviors at reloading stage. Loose sand shows stiffness increase at reloading. This phenomenon has been considered at the PZC model. Yet, dense sand sample reveals stiffness decrease and dilative behavior at reloading because of high relative density. PZC model does not show this behavior, and a modification seemed necessary. The modification proposed in this paper does not increase the number of model parameters despite most of previous modifications in which model parameters' increase made it more difficult to use. The present paper describes this modification. Drained condition is assumed at the simulations.

2 Pastor–Zienkiewicz–Chan model description [18, 33]

The PZC model is defined in *p*-*q* triaxial space. This model is formulated in p-q-θ space and subsequently is extended to three-dimensional Cartesian coordinate system that is appropriate for model implementation and numerical simulations. This model requires seven parameters at monotonic loading, one of them, α, being constant, and ten parameters at dynamic loading.

The relation between the increments of stress and strain for a material can be expressed as:

$$\dot{\sigma} = D^{\mathrm{ep}} : \dot{\varepsilon} \tag{1}$$

where $\dot{\sigma}$, $\dot{\varepsilon}$ and D^{ep} represent stress rate, strain rate and elasto-plastic tensor, respectively. The elasto-plastic tensor in generalized plasticity is as follows:

$$D^{\mathrm{ep}} = D^{\mathrm{e}} - \frac{D^{\mathrm{e}} : n_{\mathrm{gL/U}} : n^{\mathrm{T}} : D^{\mathrm{e}}}{H_{\mathrm{L/U}} + n^{\mathrm{T}} : D^{\mathrm{e}} : n_{\mathrm{gL/U}}} \tag{2}$$

where n, $n_{\mathrm{gL/U}}$ and $H_{\mathrm{L/U}}$ represent loading direction vector, plastic flow direction vector under loading and unloading condition, and plastic modulus for loading and unloading, respectively.

The elastic behavior is Hoek elasticity that defines the shear and bulk moduli (G and K), which are dependent on the stress level (p). The mean effective stress (p) is normalized by atmospheric pressure (p_a). Shear modulus and bulk modulus are expressed as:

$$G = G_0\left(\frac{p}{p_a}\right) \tag{3a}$$

$$K = K_0\left(\frac{p}{p_a}\right) \tag{3b}$$

where G_0 and K_0 represent shear and bulk modulus number and p_a atmospheric pressure that is equal to 101.325 kPa. P represents the mean stress that is expressed as $p = I_1/3$. I_1 is the first stress invariant. In (p, q, θ) space, the relations between stress rate and elastic strain rate are: $\dot{q} = 3G\dot{\varepsilon}_s$ and $\dot{p} = K\dot{\varepsilon}_v$, yet, for numerical aims, it is better to use elastic tensor in Cartesian space.

Pastor et al. [32] adopted the following generalized expression for stress–dilatancy relationship:

$$d_g = \frac{d\varepsilon_v^p}{d\varepsilon_s^p} = (1+\alpha)(M_g - \eta) \tag{4}$$

where $d\varepsilon_v^p$ and $d\varepsilon_s^p$ represent incremental plastic volumetric and plastic deviatoric strains, respectively. M_g is the slope of the critical state line on p-q plane, $\eta(= q/p)$ is the stress ratio, and α is a model parameter. M_g is dependent on the angle of internal friction at the critical state, ϕ_c, and Lode's angle, θ:

$$M_g = \frac{6\sin\phi_c}{3 - \sin\phi_c \sin 3\theta} \tag{5}$$

$$\sin 3\theta = \frac{3\sqrt{3}}{2}\frac{j_3}{\sqrt{j_2^3}} \tag{6}$$

where j_2 and j_3 represent second and third deviatoric stress invariants, respectively.

In PZC model, yield and potential surfaces are not defined explicitly. Instead, gradient vectors of these surfaces are used. Gradient vector of yield surface is known as loading direction vector, i.e., n, and gradient vector of potential surface as plastic flow direction vector, n_g.The flow rule is assumed to be nonassociated so the aforementioned two vectors are not same:

$$n = \left(\frac{\partial f}{\partial p}, \frac{\partial f}{\partial q}, \frac{\partial f}{\partial \theta}\right) = (d_f, 1, -qM_f\cos 3\theta/2) \tag{7}$$

$$n_g = \left(\frac{\partial g}{\partial p}, \frac{\partial g}{\partial q}, \frac{\partial g}{\partial \theta}\right) = (d_g, 1, -qM_g\cos 3\theta/2) \tag{8}$$

where f and g represent yield and plastic potential surfaces, respectively, M_f is a model parameter and $d_f = (1+\alpha)(M_f - \eta)$.

By choosing $M_f = M_g$, an associated plasticity model can be produced. Pastor et al. [33] suggested using the approximate relation $M_f/M_g = D_r$ in order to estimate M_f in granular materials. It is worth noting that M_f/M_g ratio should be constant.

The plastic modulus during virgin loading is as follows:

$$H_L = H_0 p H_f\{H_v + H_s\} \tag{9}$$

$$H_f = (1 - \eta/\eta_f)^4 \tag{10}$$

$$\eta_f = (1 + 1/\alpha)M_f \tag{11}$$

$$H_v = 1 - \eta/M_g \tag{12}$$

$$H_s = \beta_0\beta_1\exp(-\beta_0\xi) \tag{13}$$

where H_L represents the plastic modulus in loading, H_0 the plastic modulus number, and H_f, H_v and H_s the plastic coefficients. η_f is the stress ratio parameter. β_0 and β_1 are material model constants, and ξ is the accumulated plastic deviatoric strain: $\xi = \int |d\varepsilon_s^p|$.

The reloading plastic modulus H_L is given by:

$$H_L = H_0 p H_f\{H_v + H_s\}H_{DM} \tag{14}$$

where H_{DM} is a discrete memory factor defined by:

$$H_{DM} = \left(\frac{\zeta_{max}}{\zeta}\right)^{\gamma} \tag{15}$$

where γ is a model constant that has to be calibrated to provide the best prediction of loading–reloading experiments. γ changes at the range of 1.0–15.0. ζ is a mobilized stress function defined by:

$$\zeta = p\left(1 - \frac{\alpha}{1+\alpha}\frac{\eta}{M_f}\right)^{-1/\alpha} \tag{16}$$

Therefore, the discrete memory factor, H_{DM}, is unity during virgin loading. Reloading takes place by a higher plastic modulus with respect to the virgin loading. As observed in drained cyclic triaxial experiments by Pradhan et al. [35], dense sands show lower stiffness at reloading rather than at virgin loading. The present model is not able to reveal this phenomenon because H_{DM} is always equal or more than unity. To take into account stiffness decrease in dense sand at reloading, it is useful to define H_{DM} somehow be able to distinguish between loose and dense state and assume for to be in the range of $0.0 < H_{DM} \leq 1.0$. For this aim, γ in Eq. 15 should be a negative value. Plastic modulus, H_L, in Eq. 14 is decreased at reloading with respect to virgin loading by multiplying the new H_{DM} by

H_L. The proposed modification will be discussed in more detail in the next section.

Plastic modulus during unloading is defined by H_u as follows:

$$H_u = H_{u0}\left(M_g/\eta_u\right)^{\gamma_u} \quad \text{for } \left|M_g/\eta_u\right| > 1 \tag{17a}$$

$$H_u = H_{u0} \quad \text{for } \left|M_g/\eta_u\right| \le 1 \tag{17b}$$

where γ_u is a model constant, H_{u0} is unloading plastic modulus number, and η_u is the stress ratio from which unloading takes place. To determine the direction of plastic flow produced during unloading, it should be noted that irreversible strains are of a contractive (densifying) nature. The direction n_{gu} can thus be provided by:

$$n_{\text{gu}} = \left(n^p_{\text{gu}}, n^q_{\text{gu}}, n^\theta_{\text{gu}}\right)^T = \left(\left|n^{\text{p}}_{\text{gL}}\right|, n^{\text{q}}_{\text{gL}}, n^\theta_{\text{gL}}\right)^T \tag{18}$$

Indices u and L indicate unloading and loading conditions. As observed above, volumetric component of n_{gu}, i.e., $\left|n^{\text{p}}_{\text{gL}}\right|$, is always positive, which is indicative of the contractive nature of volumetric plastic strain (compression is assumed positive). n_{u} is the same as n vector in loading:

$$n_{\text{u}} = \left(n^{\text{p}}_{\text{u}}, n^{\text{q}}_{\text{u}}, n^\theta_{\text{u}}\right)^{\text{T}} = \left(n^{\text{p}}_{\text{L}}, n^{\text{q}}_{\text{L}}, n^\theta_{\text{L}}\right)^{\text{T}} \tag{19}$$

2.1 Transforming PZC model from p, q, θ space to Cartesian 3D space [53]

To implement the constitutive models simply, it is useful to transform the model to the general 3D space that requires formulation of vectors n and n_{g} at the latter space. The transformation procedure of the vector n_{g} is the same as $\boldsymbol{n}$, but g and M_{g} are used instead of f and M_{f}, respectively. n can be expressed in terms of I_1, J_2 and θ in the below form:

$$\begin{aligned} n &= \frac{\partial f}{\partial \sigma} = \frac{\partial f}{\partial p}\frac{\partial p}{\partial \sigma} + \frac{\partial f}{\partial q}\frac{\partial q}{\partial \sigma} + \frac{\partial f}{\partial \theta}\frac{\partial \theta}{\partial \sigma} \\ &= \frac{\partial f}{\partial I_1}\frac{\partial I_1}{\partial \sigma} + \frac{\partial f}{\partial J_2}\frac{\partial J_2}{\partial \sigma} + \frac{\partial f}{\partial \theta}\frac{\partial \theta}{\partial \sigma} \end{aligned} \tag{20}$$

After some rearrangements, the expression for $\boldsymbol{n}$ is:

$$\begin{aligned} n &= B_1 n_1 + B_2 n_2 + B_3 n_3 \\ &= \frac{\partial f}{\partial I_1}\frac{\partial I_1}{\partial \sigma} + \left(\frac{\partial f}{\partial \sqrt{J_2}} - \frac{\tan 3\theta}{\sqrt{J_2}}\frac{\partial f}{\partial \theta}\right)\frac{\partial \sqrt{J_2}}{\partial \sigma} \\ &\quad + \frac{\sqrt{3}}{2\cos 3\theta}\frac{1}{J_2^{3/2}}\frac{\partial J_3}{\partial \sigma}\frac{\partial f}{\partial \theta} \end{aligned} \tag{21}$$

Component description of vector $\boldsymbol{n}$ is:

$$n_1 = \frac{\partial I_1}{\partial \sigma} = \{1, 1, 1, 0, 0, 0\}^T \tag{22a}$$

$$n_2 = \frac{\partial \sqrt{J_2}}{\partial \sigma} = \frac{1}{2\sqrt{J_2}}\{s_{11}, s_{22}, s_{33}, 2s_{12}, 2s_{13}, 2s_{23}\}^T \tag{22b}$$

$$n_3 = \frac{\partial J_3}{\partial \sigma} = \begin{bmatrix} s_{22}s_{33} - s_{23}^2 + J_2/3 \\ s_{33}s_{11} - s_{31}^2 + J_2/3 \\ s_{11}s_{22} - s_{12}^2 + J_2/3 \\ 2(s_{13}s_{12} - s_{11}s_{23}) \\ 2(s_{12}s_{23} - s_{22}s_{13}) \\ 2(s_{12}s_{23} - s_{22}s_{13}) \end{bmatrix} \tag{22c}$$

$$B_1 = \frac{\partial f}{\partial I_1} = \frac{df}{3} \tag{23a}$$

$$B_2 = \left(\frac{\partial f}{\partial \sqrt{J_2}} - \frac{\tan 3\theta}{\sqrt{J_2}}\frac{\partial f}{\partial \theta}\right) = \sqrt{3} + \frac{\sqrt{3}}{2}M_f \sin 3\theta \tag{23b}$$

$$B_3 = \frac{\sqrt{3}}{2\cos 3\theta}\frac{1}{J_2^{3/2}}\frac{\partial f}{\partial \theta} = -\frac{3}{4}\frac{M_f}{J_2} \tag{23c}$$

$s_{ij}(= \sigma_{ij} - p\delta_{ij})$ is deviator stress while δ_{ij} is Kronecker delta.

3 Proposed modification

Stress memory factor, H_{DM}, which is multiplied by plastic modulus H_L, shows stress history effect at reloading stage in the PZC model. H_{DM} is defined by Eqs. 15 and 16. Equation 16 defines the mobilized stress value by ζ. As it was discussed in the previous section, to take into account stiffness decrease at reloading of dense sands, it is necessary for H_{DM} to be at the range of $0.0 < H_{\text{DM}} \le 1.0$, and this calls for γ to be negative, while γ has positive value in the PZC model. H_{DM} value will be discussed in more detail in the following section.

At the PZC model, the maximum value of ζ is saved at the end of virgin loading and is used for H_{DM} calculation at reloading. H_{DM} is equal to 1.0 at virgin loading. At the beginning of reloading, when $\zeta < \zeta_{\max}$, H_{DM} exceeds unity according to Eq. 15, yet when ζ increases and its value goes above $\zeta_{\max}$, H_{DM} decreases to unity. Figure 1 shows H_{DM} in the PZC model versus shear strain at the first reloading of a drained dynamic triaxial test simulation in dense sand.

Loose sands reveal densifying nature, and plastic modulus increases during drained dynamic reloading. Therefore, defined H_{DM} in the PZC model is more appropriate for loose sands. Dense sand becomes softer and has lower stress–strain slope at reloading compared with slope at virgin loading, so defined H_{DM} in the PZC model does not show the stiffness degradation behavior.

To subject stiffness degradation of dense sand at reloading, H_{DM} value must be between 0.0 and 1.0, further, and a negative value is required for γ. An expression is needed to be multiplied by γ in Eq. 15 to change the power of $(\zeta_{\max}/\zeta)$ to a negative value. This expression must be capable of distinguishing loose and dense state of sand. A

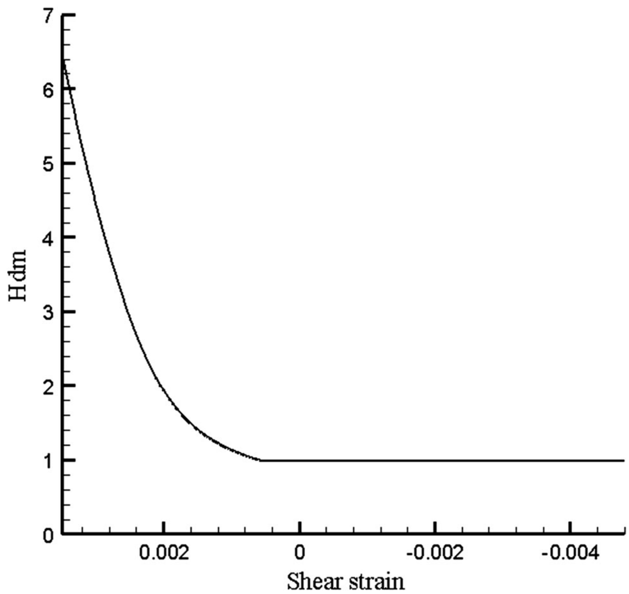

Fig. 1 H_{DM} versus shear strain at extension reloading of dense sand using the PZC model

new model constant, γ', is preferred to replace γ. Hence, the following relation for modified H_{DM} is introduced:

$$H_{DM} = \left(\frac{\zeta_{max}}{\zeta}\right)^{\gamma'\left(0.5 - M_f/M_g\right)} \tag{24}$$

Taking this expression and possible M_f/M_g values for sands into account, the range of γ changes from 1.0 $\sim$ 15.0 at the PZC model to 1.0 $\sim$ 400.0 at the modified PZC model. Pastor et al. [8] reported that M_f/M_g ratio could be equal to relative density (D_r). The expression $\left(0.5 - M_f/M_g\right)$ in Eq. 24 shows loose or dense state of sand. Common range for the relative density of granular materials is from 0.3 to 0.7. Therefore, 0.5 is taken as the average relative density and M_f/M_g as the relative density of sand (D_r). According to the above assumption, when a dense sand is simulated, the expression $\left(0.5 - M_f/M_g\right)$ is negative and by multiplying it by γ', the power of Eq. 24 is negative; therefore, H_{DM} will be lower than unity, and by multiplying H_{DM} by H_L, in Eq. 14, plastic modulus decreases at reloading. When loose sand is simulated, the expression $\left(0.5 - M_f/M_g\right)$ is positive and the power of Eq. 24 is also positive. Therefore, H_{DM} will be equal to or more than unity, which is indicative of the fact that the stiffness increases for loose sand at reloading. $\gamma'\left(0.5 - M_f/M_g\right)$ value (in the modified PZC model) for loose sand could be equal to γ (in the PZC model) via calibration in the PZC model. As observed, the proposed modification only modifies dynamic behavior of dense sand.

Using the modified PZC model, at the beginning of dense sand reloading, mobilized stress (ζ) value is lower and therefore, modified H_{DM} should be a positive value lower than unity. When mobilized stress value increases by loading progress and exceeds the previous ξ_{max} value, H_{DM} increases and reaches its maximum value, i.e., 1.0. Figure 2 shows modified H_{DM} versus shear strain at the first reloading of a drained dynamic triaxial test simulation in dense sand.

The proposed modification shows better agreement with the experimental results. Four simulations of dynamic loading will be introduced in the following sections.

4 Simulation of drained cyclic test by the PZC and modified PZC models

Two drained dynamic triaxial tests, one by Tatsuaka et al. [40] on loose sand and another by Pradhan et al. [35] on dense sand, as well as two drained dynamic plane strain tests on dense sand by Masuda et al. [24] are simulated using the PZC model and the modified PZC model. Simulations of loose sand test by two models reveal the same results. Indeed, the proposed scheme does not promote simulation of loose sand; yet, it produces better results with respect to the PZC model for dense sand.

4.1 Loose sand

4.1.1 Simulation of Tatsuoka and Ishihara tests

Tatsuoka and Ishihara [40] conducted a series of drained cyclic triaxial tests on Fuji river sand. Void ratio at the

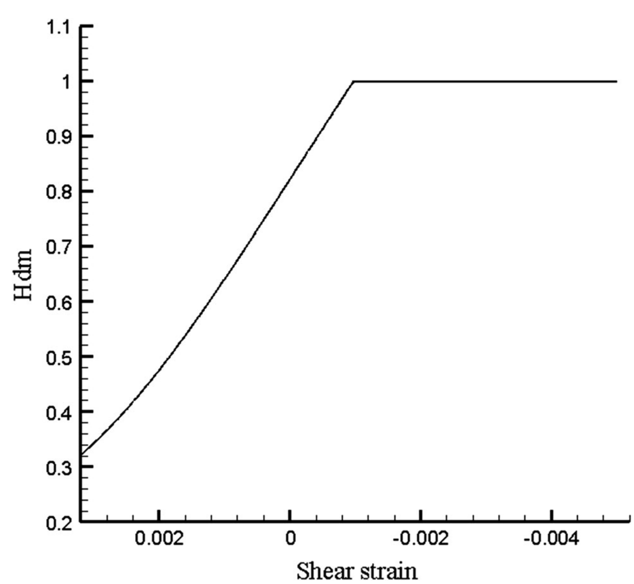

Fig. 2 Modified H_{DM} versus shear strain at the extension reloading of dense sand

Table 1 Parameters of the PZC model and the modified PZC model used for simulation of drained cyclic triaxial test

K_0	G_0	M_f	M_g	H_0	H_{0u}	β_0	β_1	α	γ'[a]	γ'[b]	γ_u
2e4	8e3	0.6	1.4	8e2	2e3	5.0	0.2	0.45	1.0	14.0	10

[a] PZC only

[b] Modified PZC only

beginning of the test was 0.74, which indicates relatively loose sand. Confining pressure was 200 kPa. Shear strain definition in this test is $\gamma(=\varepsilon_a-\varepsilon_r)$ where ε_a is axial strain and ε_r is radial strain. Model parameters at the PZC model are presented in Table 1.

Figure 3 illustrates stress–strain curve in drained cyclic triaxial test, and Fig. 4 illustrates stress–strain curve by simulation without any modifications. M_f/M_g is equal 0.43 at this simulation, which indicates a relatively loose sand in terms of the proposed modification scheme. Power value of H_{DM} equation at the PZC model (γ) by calibration is equal to 1.0 to fit the experimental results best and at the modified model is: $\gamma'(0.5-M_f/M_g)=0.07\gamma'$. By assuming 14.0 for γ', $\gamma'(0.5-M_f/M_g)$ becomes 1.0 and reloading curve best fits to the experiment (Fig. 3), i.e., the modification method does not work for sands with M_f/M_g value lower than 0.5.

4.2 Dense sand

4.2.1 Simulation of Pradhan et al. tests

Pradhan et al. [35] carried out a series of cyclic constant-p triaxial tests on saturated Toyoura sand under drained

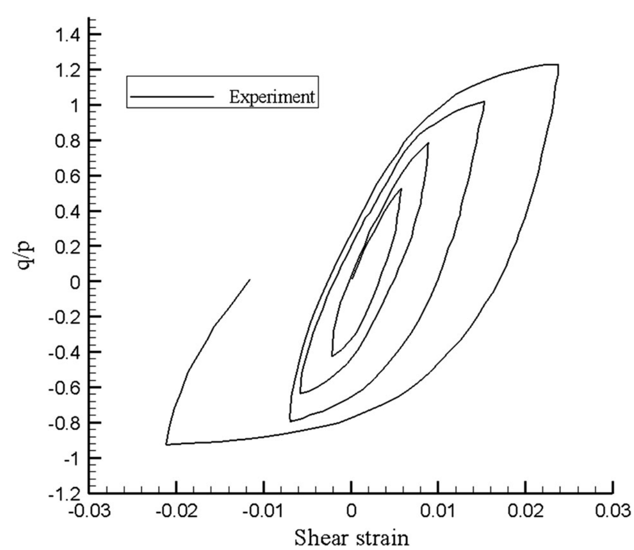

Fig. 3 Results of drained cyclic triaxial test for loose sand, stress ratio versus shear strain (experiments from Tatsuoka and Ishihara [40])

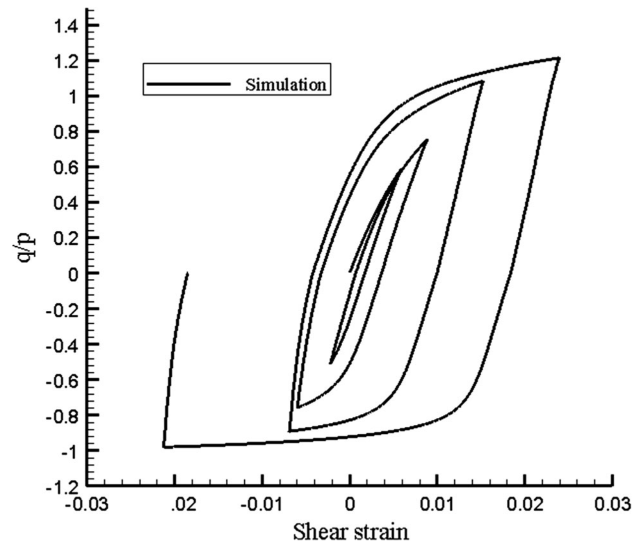

Fig. 4 Simulation of drained cyclic triaxial test on loose sand, stress ratio versus shear strain, by the PZC model and the modified PZC model (the curves of two simulations overlap on each other)

condition. P represents the mean effective stress. The physical properties of Toyoura sand are $G_s=2.64, D_{50}=0.16$ mm, $U_c=1.46, e_{max}=0.977, e_{min}=0.605$, and fine contents less than 74 μm are not included. The mean effective stress value is 98.1 kPa. Shear strain at this test is: $\gamma(=\varepsilon_a-\varepsilon_r)$. The selected test number for simulation is CYCD09. Initial void ratio is $e_0=0.653$, which indicates dense sand. Parameters of the simulation are presented at Table 2.

Figure 5 shows the experimental results of the test. Figure 6 shows two simulations of this test, one by the PZC model and another by the modified PZC model. The modified model illustrates lower stiffness at reloading of compression and extension compared with the virgin loading. This is because H_{DM} is lower than unity at reloading compared with its value at virgin loading and consequently plastic modulus is lower at reloading compared with plastic modulus at virgin loading. The simulation by the PZC model does not show this behavior. γ' is taken 30.0 at the modified model. Other parameters of the modified PZC model are the same as for the PZC model.

4.2.2 Simulation of Masuda et al. tests

Masuda et al. [24] studied cyclic stress–strain behavior of dense sand in a conventional plane strain apparatus. They used Toyoura sand for the plane strain tests. The mean grain size, D_{50}, is 0.162 mm, the uniformity coefficient, U_c, is 1.46, the minimum void ratio, e_{min}, is 0.612, the maximum void ratio, e_{max}, is 0.973, and the specific gravity, G_s, is 2.64. Specimens were prepared by pluviating air-dried sand particles. A series of cyclic loading tests were conducted at a constant pressure σ_h, where σ_h is

Table 2 Parameters of the PZC model and the modified PZC model used for simulation of drained cyclic triaxial test

K_0	G_0	M_f	M_g	H_0	H_{0u}	β_0	β_1	α	γ[a]	γ'[b]	γ_u
8.5e4	2.5e4	0.68	1.25	3e3	5e3	7.0	0.15	0.45	1.0	30.0	15

[a] PZC only

[b] Modified PZC only

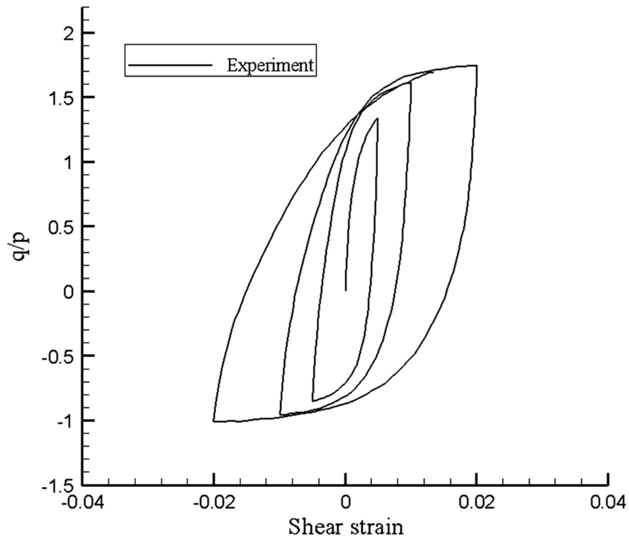

Fig. 5 Drained constant-p cyclic triaxial test on dense sand, stress ratio versus shear strain (experiments from Pradhan et al. [35])

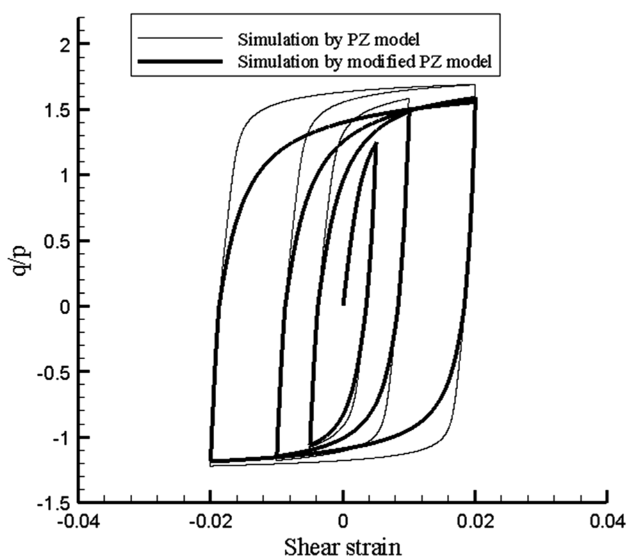

Fig. 6 Simulation of the drained cyclic triaxial test on dense sand by the PZC model and the modified PZC model, stress ratio versus shear strain

horizontal pressure. Some of specimens were consolidated isotropically with an initial stress state $\sigma_\mathrm{h} = \sigma_\mathrm{v} = 78.5$ kPa, and others were consolidated anisotropically with an initial stress state of $\sigma_\mathrm{h} = 78.5$ kPa and $\sigma_v = 29.5$kPa. The specimen's dimensions are 20 cm at

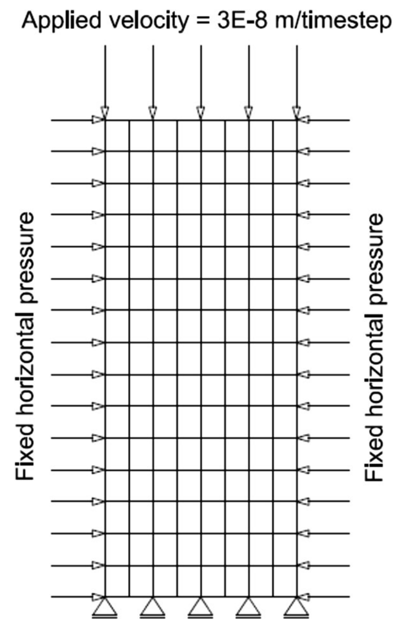

Fig. 7 The meshing and boundary conditions for simulation of plane strain test

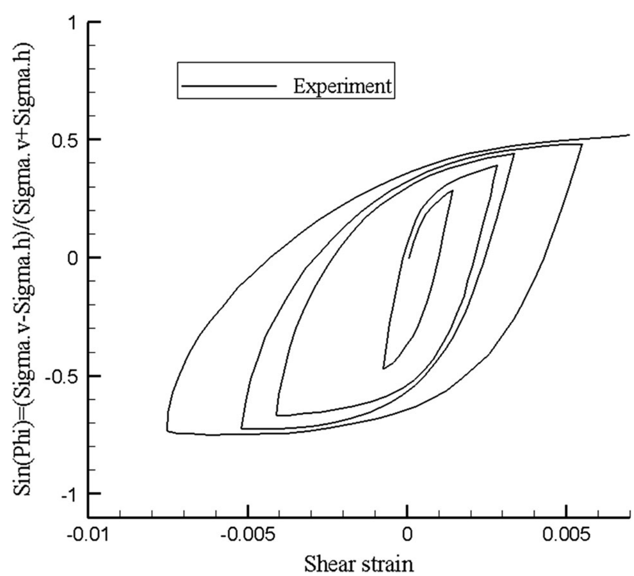

Fig. 8 Cyclic loading test on isotropically consolidated specimen, case 5–6, relationship between $\sin\varphi_{\mathrm{mob}} = (\sigma_v - \sigma_h)/(\sigma_v + \sigma_h)$ and shear strain $\gamma = \varepsilon_v - \varepsilon_h$, initial state: $\sigma_h = \sigma_v = 78.5$ kPa and $e_0 = 0.654$ (experiment from Masuda et al. [24])

Table 3 Parameters of the modified PZC and the PZC model used for simulations of drained cyclic plane strain tests

Cases	K_0	G_0	M_f	M_g	H_0	H_{0u}	β_0	β_1	α	γ[a]	γ'[b]	γ_u
Cases 5–6	40e3	30e3	0.9	1.2	4e3	1e4	4.0	0.1	0.45	1.0	2.0	1.0
Cases 2–5	42e3	43e3	0.95	1.1	1.5e3	1e4	10.0	0.1	0.45	1.0	1.0	15.0

[a] PZC only

[b] Modified PZC only

height, σ_v direction, 16 cm at length and 8 cm at width, σ_h direction. The results are presented in terms of mobilized friction angle, $\sin\varphi_{mob} = (\sigma_v - \sigma_h)/(\sigma_v + \sigma_h)$, and shear strain, $= \varepsilon_v - \varepsilon_h$.

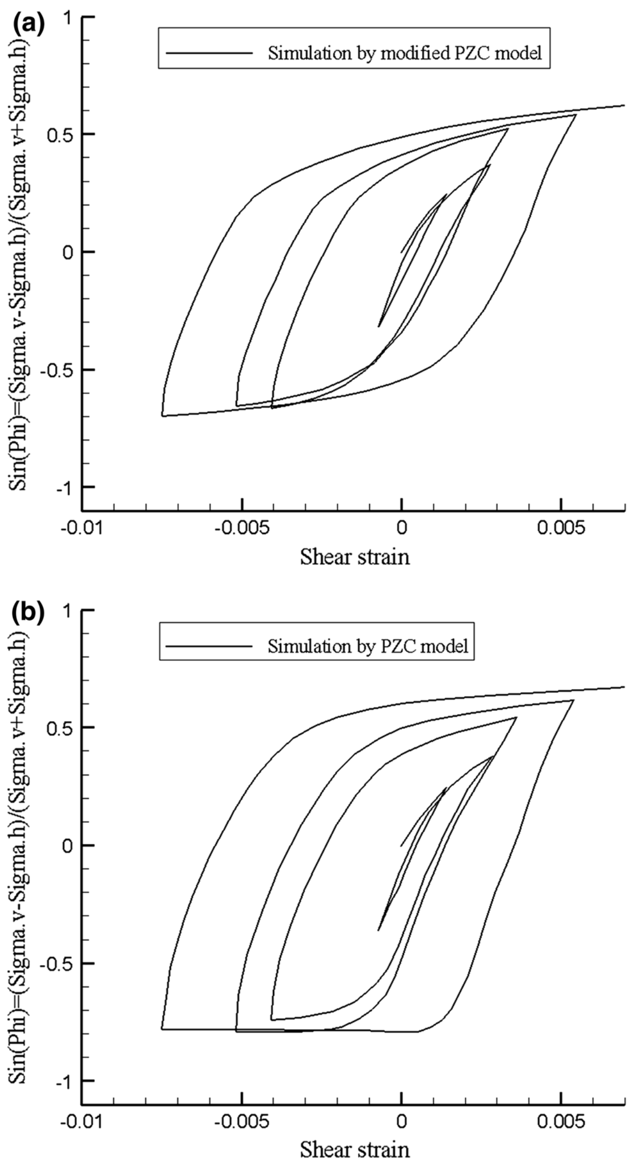

Fig. 9 Simulations of cyclic loading test on isotropically consolidated specimen, case 5–6, relationship between $\sin\varphi_{mob} = (\sigma_v - \sigma_h)/(\sigma_v + \sigma_h)$ and shear strain $= \varepsilon_v - \varepsilon_h$, **a** simulation by the modified PZC model, **b** simulation by the PZC model

Two cyclic plane strain tests (cases 5–6 and 2–5) are simulated and compared with the experiments. Both the modified PZC model and the PZC model are implemented in a finite difference code. A finite difference mesh is constructed by 15 zones at height and eight zones at width. The meshing system, including boundary conditions, is illustrated in Fig. 7. The model is fixed at the end bottom nodes along vertical direction. A constant horizontal pressure, 78.5 kPa for isotropically consolidated specimen (case 5–6) and 29.5 kPa for anisotropically consolidated specimen (case 2–5), is applied to the left and right nodes during loading. A constant rate of velocity, 3E − 8 m/time step, is maintained at the top nodes along vertical direction toward the bottom.

The model parameters for the modified PZC model and the PZC model in the two cases, extracted via calibration of the experimental results, are presented in Table 3.

The results of cyclic tests for cases 5–6 and 2–5 are shown in Figs. 8 and 10, respectively. Case 5–6 was consolidated isotropically with the initial state: $\sigma_h = \sigma_v = 78.5$ kPa and $e_0 = 0.654$, and case 2–5 was consolidated anisotropically with the initial state: $\sigma_h = 78.5$ kPa, $\sigma_v =$

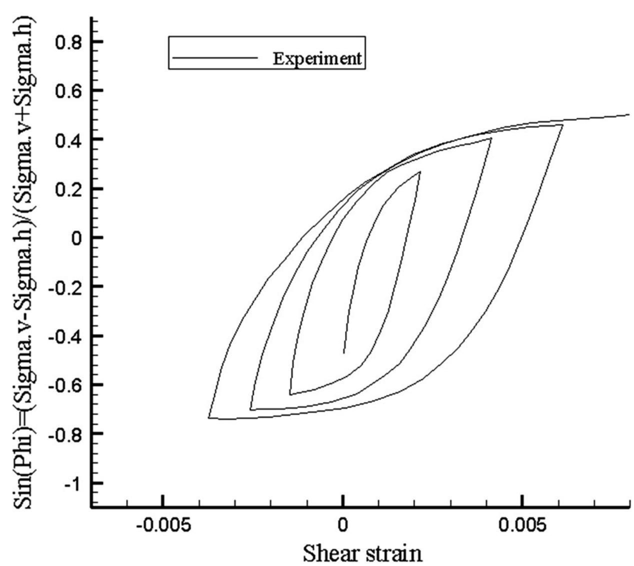

Fig. 10 Cyclic loading test on anisotropically consolidated specimen, case 2–5, relationship between $\sin\varphi_{mob} = (\sigma_v - \sigma_h)/(\sigma_v + \sigma_h)$ and shear strain $\gamma = \varepsilon_v - \varepsilon_h$, initial state:$\sigma_h = 78.5kPa, \sigma_v = 29.5kPa$ and $e_0 = 0.659$ (experiment from Masuda et al. [24])

29.5 kPa and $e_0 = 0.659$. Calculation of relative density for both tests reveals high relative density values that indicate dense specimens. The calibrated values of M_f and M_g and their ratio also indicate dense state.

Both cyclic tests show stiffness degradation at reloading (Figs. 8, 10). As observed, simulation curves by the modified PZC model present stiffness decrease at the reloading stages of compression and extension in Figs. 9 and 11. γ is taken 1.0 for the PZC model in both cases. Therefore, stress memory factor becomes $H_{DM} = (\zeta_{max}/\zeta)^{\gamma} = (\zeta_{max}/\zeta)$. This indicates that H_{DM} always exceeds unity and plastic modulus, H_L, captures high values at reloading stages. Simulation curves by the PZC model in Figs. 9b and 11b represent this trend. γ' is taken 2.0 for case 5–6 and 1.0 for case 2–5. Modified stress memory factor becomes $H_{DM} = (\zeta_{max}/\zeta)^{\gamma'(0.5-M_f/M_g)} = (\zeta_{max}/\zeta)^{-0.5}$ for case 5–6 and $H_{DM} = (\zeta_{max}/\zeta)^{-0.36}$ for case 2–5. It can be inferred that H_{DM} will change at the range of $0.0 < H_{DM} \leq 1.0$, and consequently, plastic modulus takes lower values compared with its values at the PZC model. The slopes of the reloading curves tend to decrease compared with the slopes at virgin loading as can be seen in Figs. 9a and 11a.

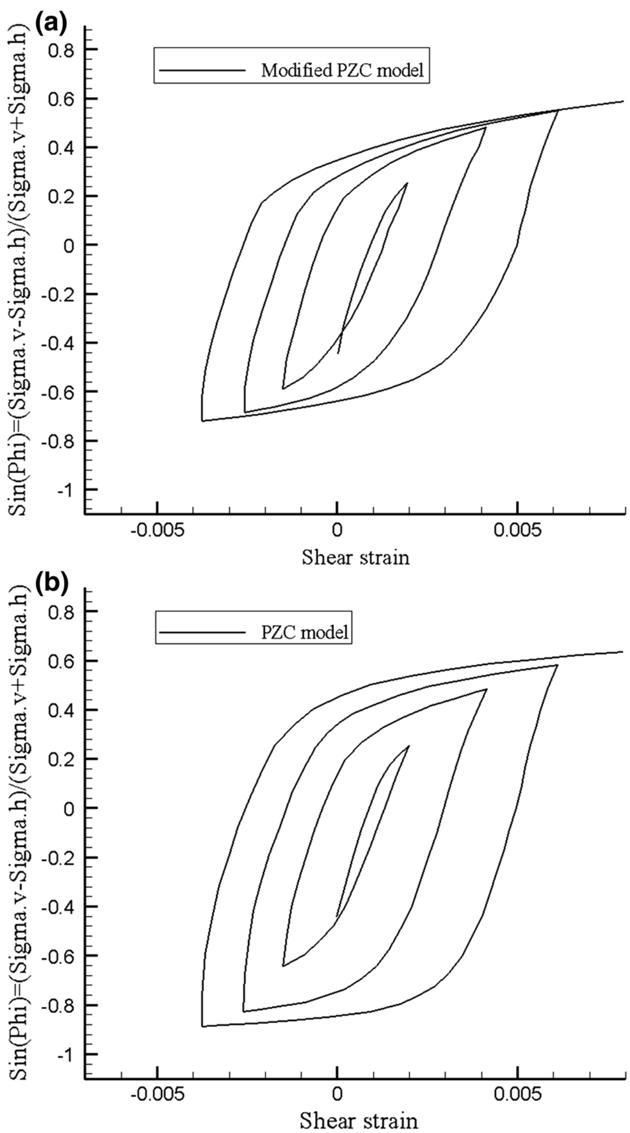

Fig. 11 Simulations of cyclic loading test on anisotropically consolidated specimen, case 2–5, relationship between $\sin\varphi_{mob} = (\sigma_v - \sigma_h)/(\sigma_v + \sigma_h)$ and shear strain $= \varepsilon_v - \varepsilon_h$, **a** simulation by the modified PZC model, **b** simulation by the PZC model

5 Conclusions

The PZC model is a suitable constitutive model based on the generalized plasticity and the concept of the yield surface gradient vectors. This model has been mainly used with the aim of simulating saturated sand under undrained condition. In order to improve its prediction for the dynamic behavior of dense sand, a modification is introduced by considering stiffness degradation under dynamic loading and drained condition.

The PZC model includes a stress memory factor (H_{DM}) that considers only stiffness increase behavior at reloading. This model needs to take the stiffness decrease in dense sand at reloading stages of dynamic loading into account. A simple modification to H_{DM} is made to simulate the stiffness degradation of dense sand at reloading. The proposed modification does not increase the number of model parameters.

Two cyclic triaxial tests on dense and loose sand and two relatively large-scale plane strain cyclic tests on dense sand are simulated by the PZC model and the modified PZC model. It is indicated that the proposed modification is useful for simulating cyclic behavior of dense sand. Stress–strain curves of all modified simulations present stiffness degradation of dense sand at reloading stages of compression and extension as well.

References

1. Bahda F, Pastor M, Saitta A (1997) A double hardening model based on generalized plasticity and state parameters for cyclic loading of sands. In: Pietruszczak S, Pande GN, Balkema AA (eds) Numerical models in Geomechanics. The Netherlands, Rotterdam, pp 33–38
2. Bolzon G, Schrefler BA, Zienkiewicz OC (1996) Elastoplastic soil constitutive laws generalized to partially saturated states. Geotechnique 46(2):279–289
3. Chambon R (1989) Une classe de lois de compartement incrementelement non lineaire pour les sols non visqueux, resolution de quelques problemes de coherences. C R Acad Sci 308:1571–1576

4. Chambon R (2001) Incremental behaviour of a simple deviatoric constitutive CLoE model. In: Mühlhaus HB et al (eds) Bifurcation and localization theory in geomechanics. Lisse, Swets, pp 21–28
5. Cola S, Tonni L (2007) Adapting a generalized plasticity model to reproduce the stress-strain response of silty soils forming the Venice lagoon basin. In: Geomechanics: laboratory testing, modeling and applications. A collection of papers of the geotechnical symposium in Rome, Springer, (16–17 March 2006), 146: 743–756
6. Cola S, Tonni L, Pastor M (2008) Mathematical modelling of venetian sediment behaviour using generalized plasticity. In: 12th conference of the Int Assoc for Computer Meth and Advances in Geomechanics (IACMAG), Goa, 1–6 Oct, pp 838–846
7. Darve F, Flavigny E, Rojas E (1986) A class of incrementally non-linear constitutive relations and applications to clays. Comput Geotech 2:43–66
8. Darve F, Flavigny E, Megachou M (1995) Yield surfaces and principle of superposition revisited by incrementally non-linear constitutive relations. Int J Plast 11(8):927–948
9. Desrues J, Chambon R (1989) Shear band analysis for granular materials: the question of incremental non-linearity. Ingenieur–Archiv 59:187–196
10. Merodo JA, Tamagnini R, Pastor M, Mira P (2005) Modelling damage with generalized plasticity. Rivista Italiana di Geotecnica 4:32–42
11. Fuentes W, Triantafyllidis T, Lizcano A (2012) Hypoplastic model for sands with loading surface. Acta Geotech 7:177–192
12. Gudehus G (1996) A comprehensive constitutive equation for granular materials. Soils Found 36(1):1–12
13. Gudehus G (2004) A visco-hypoplastic constitutive relation for soft soils. Soils Found 44(4):11–25
14. Herle I, Kolymbas D (2004) Hypoplasticity for soils with low friction angles. Comput Geotech 31(5):365–373
15. Kolymbas D (1978) Eine konstitutive Eine konstitutive Theorie fur Boden und andere kormige Stoffe. PhD thesis, Karlsruhe University, Germany
16. Kolymbas D (1991) Computer-aided design of constitutive laws. Int J Numer Anal Methods Geomech 15:593–604
17. Lanier J, Caillerie D, Chambon R (2004) A general formulation of hypoplasticity. Int J Numer Anal Meth Geomech 28(15): 1461–1478
18. Ling HI, Liu H (2003) Pressure-level dependency and densification behavior of sand through generalized plasticity model. J Eng Mech 129(8):851–860
19. Ling HI, Yang S (2006) Unified sand model based on the critical state and generalized plasticity. J Eng Mech 132(12):1380–1391
20. Liu H, Ling HI (2008) Constitutive description of interface behavior including cyclic loading and particle breakage within the framework of critical state soil mechanics. Int J Numer Anal Meth Geomech 32:1495–1514
21. Manzanal D, Merodo AF, Pastor M (2010) Generalized plasticity state parameter-based model for saturated and unsaturated soils. Part 1: Saturated state. Int J Numer Anal Meth Geomech. DOI: 10.1002/nag
22. Mašín D (2005) A hypoplastic constitutive model for clays. Int J Numer Anal Methods Geomech 29:311–336
23. Mašín D (2012) Clay hypoplasticity with explicitly defined asymptotic states. Acta Geotech. doi:10.1007/s11440-012-0199-y
24. Masuda T, Tatsuoka F, Yamada Sh, Sato T (1999) Stress-strain behavior of sand in plain strain compression, extension and cyclic loading tests. Soils Found 39(5):31–45
25. Mira P, Tonni M, Pastor M, Fernandez Merodo A (2009) A generalized midpoint algorithm for the integration of a generalized plasticity model for sands. Int J Numer Meth Eng 77:1201–1223
26. Mroz Z, Zienkiewicz OC (1984) Uniform formulation of constitutive equations for clays and sand. In: Mechanics of engineering materials, Desai CS, Gallagher RH (eds) Chapter 22, Wiley, New York 415–459
27. Niemunis, A (1993) Hypoplasticity vs. elasto-plasticity. Selected topics. In: Kolymbas, D. (Ed.), Modern Approaches to Plasticity in Horton Greece. Balkema 277–308
28. Niemunis A (2003) Extended hypoplastic models for soils. Habilitation thesis, Ruhr-University, Bochum
29. Niemunis A, Herle I (1997) Hypoplastic model for cohesionless soils with elastic strain range. Mech Cohesive-Frict Mater 2(4):279–299
30. Osinov VA (2013) Application of a high-cycle accumulation model to the analysis of soil liquefaction around a vibrating pile toe. Acta Geotech. doi:10.1007/s11440-013-0215-x
31. Pastor M, Zienkiewicz OC (1986) A generalized plasticity, hierarchial model for sand under monotonic and cyclic loading. In: Pande GN, van Impe WF (eds) Numerical methods in geomechanics. Jackson, London, pp 131–150
32. Pastor M, Zienkiewicz OC, Leung KH (1985) Simple model for transient soil loading in earthquake analysis. II: non-associative models for sands. Int J Numer Anal Meth Geomech 9(5):477–498
33. Pastor M, Zienkiewicz OC, Chan AHC (1990) General plasticity and the modelling of soil behavior. Int J Numer Anal Meth Geomech 14:151–190
34. Pastor M, Zienkiewicz OC, Xu GD, Peraire J (1993) Modeling of sand behavior: cyclic loading, anisotropy and localization. In: Kolymbas D (ed) Modern approaches to plasticity. Elsevier, New York, pp 469–492
35. Pradhan BS, Tatsuoka m F, Sato Y (1989) Experimental stress-dilatancy relations of sand subjected to cyclic loading. Soils Found 29(1):45–64
36. Santagiuliana R, Schrefler BA (2006) Enhancing the Bolzon–Schrefler–Zienkiewicz constitutive model for partially saturated soil. Transp Porous Media 65(1):1–30
37. Sassa S, Sekiguchi H (2001) Analysis of waved-induced liquefaction of sand beds. Geotechnique 51(2):115–126
38. Schrefler BA, Zhang HW, Pastor M, Zienkiewicz OC (1998) Strain localization modeling and pore pressure in saturated sand samples. Comput Mech 22:266–280
39. Tamagnini R, Pastor M (2004) A thermodynamically based model for unsaturated soils: a new framework for generalized plasticity. In: Proceedings of the second international workshop on unsaturated soil, Naples, 1–14
40. Tatsuoka F, Ishihara K (1974) Drained deformation of sand under cyclic stresses reversing direction. Soils Found 14(3):51–65
41. Tonni, L, Cola, S, and Pastor, M (2006) A generalized plasticity approach for describing the behavior of silty soils forming the Venetian lagoon basin. In: 6th European Conference on Numer Meth in Geotech Eng. 93–99. London: Taylor and Francis
42. von Wolffersdorff P-A (1996) A hypoplastic relation for granular materials with a predefined limit state surface. Mech Cohes-Frict Mater 1:251–271
43. Wu W (1992) Hypoplastizität als mathematisches Modell zum mechanischen Verhalten granularer Stoffe. Veröffentlichungen Heft 129, Institut für Bodenmechanik und Felsmechanik der Universität Fridericiana in Karlsruhe
44. Wu W, Bauer E (1994) A simple hypoplastic constitutive model for sand. Int J Numer Anal Methods Geomech 18:833–862
45. Wu W, Kolymbas D (1990) Numerical testing of the stability criterion for hypoplastic constitutive equations. Mech Mater 9:245–253
46. Wu, W, and Kolymbas, D (2000) Hypoplasticity, then and now. in: Constitutive modelling of granular materials, Springer Verlag 57-105

47. Wu W, Bauer E, Kolymbas D (1996) Hypoplastic constitutive model with critical state for granular materials. Mech Mater 23:45–69
48. Zhang J-M, Wang G (2012) Large post-liquefaction deformation of sand, part I: physical mechanism, constitutive description and numerical algorithm. Acta Geotech 7:69–113
49. Zhang HW, Heeres OM, Borst R (2001) Implicit integration of a generalized plasticity constitutive model for partially saturated soil. Eng Comput 18(12):314–336. doi:10.1007/s10587-007-0122-0
50. Zhang HW, Sanavia L, Schrefler BA (2001) Numerical analysis of dynamic strain localization in initially water saturated dense sand with a modified generalized plasticity model. Comput Struct 79:441–459
51. Zienkiewicz OC, Mroz Z (1984) Generalized plasticity formulation and application to Geomechanics. In: Desai CS, Gallagher RH (eds) Mech Eng Mater. Wiley, London 33 655–680
52. Zienkiewicz OC, Leung KH, Pastor M (1985) Simple model for transient soil loading in earthquake analysis I Basic model and its application. Int J Num Anal Meth Geomech 9:453–476
53. Zienkiewicz OC, Chan AHC, Pastor M, Schrefler B, Shiomi T (1999) Computational Geomechanics, John Wiley and Sons